Authors for "**Hubble Space Telescope Observations of Oxygen-rich Supernova Remnants in the Magellanic Clouds. III. WFPC2 Imaging of the Young, Crab-like Supernova Remnant SNR0540-69.3.**"

(6) Harvard-Smithsonian Center for Astrophysics, Cambridge, Massachusetts
(7) Department of Physics, Middlebury College, Middlebury, VT
(8) Department of Physics and Astronomy, Rutgers University, Piscataway, NJ
(9) Visiting Astronomer, Tololo Inter-American Observatory, National Optical Astronomy Observatory
(10) Hubble Fellow

Hubble Space Telescope Observations of Oxygen-rich Supernova Remnants in the Magellanic Clouds. III. WFPC2 Imaging of the Young, Crab-like Supernova Remnant SNR0540-69.3[1]

Jon A. Morse[2,3,9], Nathan Smith[4,10], William P. Blair[5], Robert P. Kirshner[6], P. Frank Winkler[7], & John P. Hughes[8]

ABSTRACT

Hubble Space Telescope images with the Wide Field Planetary Camera 2 of the young, oxygen-rich, Crab-like supernova remnant SNR0540–69.3 in the Large Magellanic Cloud (LMC) reveal details of the emission distribution and the relationship between the expanding ejecta and synchroton nebula. The emission distributions appear very similar to those seen in the Crab nebula, with the ejecta located in a thin envelope surrounding the synchrotron nebula. The [O III] emission is more extended than other tracers, forming a faint "skin" around the denser filaments and synchrotron nebula, as also observed in the Crab. The [O III] exhibits somewhat different kinematic structure in long-slit spectra, including a more extended high-velocity emission halo not seen in images. Yet even the fastest expansion speeds in SNR 0540's halo are slow when compared to most other young supernova remnants, though the Crab nebula has similar slow expansion speeds. We show a striking correspondence between the morphology of the synchrotron nebula observed in an optical continuum filter with that recently resolved in *Chandra* X-ray images. We argue that the multi-component kinematics and filamentary morphology of the optical emission-line features likely result from magnetic Rayleigh-Taylor instabilities that form as the synchrotron nebula expands and sweeps up ejecta, as seen in the Crab nebula. Our images and spectra help to refine our understanding of SNR 0540 in several more detailed respects: they confirm the identification of Hα+[N II] in the red spectrum, they show that the systemic velocity of SNR 0540 is not significantly different from that of the LMC, and they hint at a lower Ne abundance than the Crab (potentially indicating a more massive progenitor star).

---

[1]Based on observations with the NASA/ESA *Hubble Space Telescope* obtained at the Space Telescope Science Institute, which is operated by AURA, Inc., for NASA under contract NAS5-26555.

[2]Department of Physics and Astronomy, Arizona State University, Box 871504, Tempe, AZ 85287-1504

[3]Present address: NASA-Goddard Space Flight Center, Laboratory for Observational Cosmology, Mail Code 665, Greenbelt, MD 20771; Jon.Morse@nasa.gov

[4]Center for Astrophysics and Space Astronomy, University of Colorado, 389 UCB, Boulder, CO 80309; nathans@casa.colorado.edu

[5]Department of Physics and Astronomy, Johns Hopkins University, 3400 N. Charles Street, Baltimore, MD 21218; wpb@pha.jhu.edu

[6]Harvard-Smithsonian Center for Astrophysics, 60 Garden St., Cambridge, MA 02138; kirshner@cfa.harvard.edu

[7]Department of Physics, Middlebury College, Middlebury, VT 05753; winkler@panther.middlebury.edu

[8]Department of Physics and Astronomy, Rutgers University, 136 Frelinghuysen Rd., Piscataway, NJ 08854-8019; jph@physics.rutgers.edu

[9]Visiting Astronomer, Cerro Tololo Inter-American Observatory, National Optical Astronomy Observatory, operated by the Association of Universities for Research in Astronomy, Inc., under cooperative agreement with the National Science Foundation.

[10]Hubble Fellow.

Subject headings: circumstellar matter — nebulae: individual (SNR0540–69.3) — ISM: supernova remnant

1. INTRODUCTION

The young supernova remnant 0540-69.3 (SNR 0540) in the Large Magellanic Cloud (LMC) ranks as one of the most interesting objects in the small class of young, oxygen-rich remnants. Age estimates range from ∼800–1600 years, making SNR 0540 probably the most recent predecessor to SN1987A in the LMC. In fact, SNR 0540 is located at a projected distance of only $\lesssim$400 pc from SN1987A and belongs to the same generation of stars. SNR 0540 may foreshadow SN1987A's future evolution, offering a potential link between supernova remnants and their supernova type and progenitor spectral class. Such links are needed to understand chemical enrichment caused by nucleosynthesis in massive stars and distributed by supernova explosions.

SNR 0540's resemblance to the Crab nebula is a major source of the attention it garners, linking a distant supernova to a nearby, well-studied object. SNR 0540 also merits comparison with the oxygen-rich remnant Cas A, because abundances in the ∼8″ diameter shell surrounding the pulsar (Mathewson et al. 1980) show enhanced O, S, Ar, and other heavy elements indicating their origin in the nuclear processed core of a massive exploded progenitor star (Dopita & Tuohy 1984; Kirshner et al. 1989, K89 hereafter; Caraveo et al. 1992; Mathewson et al. 1980). However, the "Crab-like" remnant SNR 0540 is unique among young, O-rich remnants in that it contains a rapidly spinning 50 msec pulsar (e.g., Seward et al. 1984; Middleditch et al. 1987) powering an extended synchrotron nebula detected from X-rays to the radio (e.g., Chanan et al. 1984; Gotthelf & Wang 2000). SNR 0540's optical nebulosity consists of an expanding shell of ∼4″ radius (r≈1 pc) radiating strongly in O and S emission lines, as well as Ar, Ni, Fe, and H and/or N (Dopita & Tuohy 1984; K89; Caraveo et al. 1998; Serafimovich et al. 2005). The optical emission is likely powered by the synchrotron nebula (K89), like the Crab, through a combination of shock heating and photoexcitation.

Here we report the results of our *Hubble Space Telescope* (*HST*) Wide Field Planetary Camera 2 (WFPC2) imaging program, showing that the comparison to the Crab nebula is strengthened through new details revealed in the high-resolution images. Additionally, a ground-based optical spectrum of SNR 0540 is highly reminiscent of an integrated spectrum of the Crab. We assume a distance of 50 kpc to SNR 0540 in this paper, where 0.″1≈7.5×10^{16} cm.

Serafimovich et al. (2004) performed a detailed analysis of the pulsar PSR B0540–69.3 astrometry and flux using images from the current data set. They measured the pulsar spectral energy distribution in the optical by meticulously accounting for the contribution of the pulsar wind nebula (PWN) to flux measurements of the pulsar. Serafimovich et al. show that with significant care in accounting for the nebular contribution, the pulsar optical spectral energy distribution follows a power law with negative slope ($F_\nu \propto \nu^{-\alpha}$, $\alpha = 1.07$), and is steeper than that deduced from previous ground-based optical measurements. These authors also measure a proper motion for the pulsar of ∼5 mas yr^{-1} along the putative PWN jet axis, but with a 50% error bar. We note that new imaging with *HST* could double the time baseline of these observations, significantly decreasing the uncertainty in this difficult measurement.

2. OBSERVATIONS AND DATA REDUCTION

We observed SNR 0540 with the Planetary Camera (PC) of the *HST* WFPC2 on 17 October 1999 through the F336W, F502N, F547M, F673N, and F791W filters. We also culled additional images of SNR 0540 from the *HST* archive obtained through the F555W, F656N, and F658N filters on 19 October 1995. Table 1 provides an observing log of the exposure times through each filter. The $\sim 8''$ diameter optical emission shell was centered on the PC chip, and emission from the surrounding environment was captured on the adjacent Wide Field (WF) camera chips.

Details of our WFPC2 observing and data reduction procedures are described in Morse et al. (1996; Paper 1) and Blair et al. (2000; Paper 2). Using IRAF/STSDAS[11] software tasks, the pipeline-calibrated exposures through each filter were carefully checked for alignment and combined to reject cosmic rays as described in Paper 1. Stray hot and dead pixels were then flagged and corrected. Each chip was corrected for geometric distortions using the Trauger wavelength-dependent coefficients in the STSDAS.DITHER package and then flux calibrated using the methods described in the WFPC2 Instrument Handbook (Biretta et al. 2002).

We wished to compare the images at full PC resolution to study small-scale structure in the optical SNR, and also at the $0\farcs1$ resolution of the WF chips over the entire WFPC2 field of view for studying the local environment and to search for optical evidence of the outer SNR shell that has been detected in the X-rays (Gotthelf & Wang 2000). To do so we needed to rotate and align all the images from both epochs to a common reference frame, since the 1995 and 1999 data sets had slightly different absolute pointings and spacecraft orientations. First, the PC images were individually rotated, based on the pointing information provided in the science data header, so that north was toward the top. All the PC images were then translated to align with the F547M image using 6 – 15 common stars (depending on the filter) as tie points.

To build the larger image mosaics of the entire WFPC2 field of view, we similarly rotated each individual chip and then aligned them using the 1999 F547M image as reference. We found in this program and a complementary WFPC2 imaging program of the Cas A SNR (Fesen et al. 2001) that using the STSDAS task WMOSAIC yielded measurable errors in the inter-chip rotations and offsets. In attempting to align the WMOSAIC'ed images from the two epochs, once the stars on the WF2 chip were aligned, then the stars on the other WF chips did not precisely align. We therefore independently determined the inter-chip rotations and offsets. The different absolute pointings resulted in several stars observed in the 1995 F555W image moving across the chip boundaries in the slightly displaced 1999 F547M image. We then pieced together mosaics of the WF images chip by chip for both epochs which were aligned to a common reference frame. Finally, we re-scaled the PC images by a factor of 0.4555 so that the pixel scale agreed with the WF pixel scales and inserted the re-scaled PC images into their appropriate positions in the image mosaics for each filter. The resulting images are discussed in §3.

We also present supporting optical spectroscopic observations of SNR 0540 from the 4-meter Blanco telescope of the Cerro Tololo Inter-American Observatory using the R-C spectrograph. The R-C spectrograph data were obtained on 17 August 1995 with the KPGL3 grating used in first-order to cover the wavelength range 3335 – 6945 Å on the Loral 3k × 1k CCD. The dispersion was 1.2 Å pixel^{-1} and the spatial scale along the slit was $0\farcs52$ pixel^{-1}. We employed a $2''$ wide slit oriented at P.A.=124°. Comparing the stars observed

[11]IRAF is distributed by the National Optical Astronomy Observatories, which is operated by the Association of Universities for Research in Astronomy, Inc. (AURA) under cooperative agreement with the National Science Foundation. The Space Telescope Science Data Analysis System (STSDAS) is distributed by the Space Telescope Science Institute.

in the long-slit spectra with the WFPC2 mosaic images, the center of the slit crossed about 1″ west of the pulsar in the middle of the optical remnant (see below). The seeing was estimated at $\sim$ 1.″5 at the telescope. The full width at half maximum (FWHM) spectral resolution measured from several unresolved emission lines from the surrounding HII region was 3.5-4 pixels or $\sim$ 250 km s^{-1}. Two spectra were obtained, to recognize cosmic rays, for a total exposure time of 2700 s. We followed standard IRAF reduction procedures for flat-fielding, calibrating the slit illumination response, and wavelength calibrating the data. Several spectrophotometric standard stars were observed during the night for flux calibration. Sky subtraction was achieved by fitting a low-order polynomial to background regions adjacent to the SNR. Some strong H II region lines (e.g., Hα) had variable intensities along the slit, which made precise subtraction difficult at some wavelengths. Finally, a one-dimensional spectrum was extracted over the detector rows that subtended emission from the entire SNR. Spectroscopy of SNR 0540 is discussed in §4.

3. WFPC2 IMAGING OF THE NEBULAR COMPONENT

Figure 1 shows the WFPC2 images of SNR 0540 at the full resolution of the PC chip ($\sim$0.″046 pixel^{-1}), and Figure 2 displays the larger [S II] WFPC2 mosaic at WF resolution ($\sim$ 0.″1 pixel^{-1}). A preliminary analysis of these data was presented by Morse (2003). The optical remnant subtends about 8″ diameter, though for the first time *HST* enables us to discern morphological intricacies in the emission-line shell and synchrotron nebula.

When interpreting the emission structure, it is important to bear in mind the wavelength ranges captured in each image, especially for the narrowband filters. K89 measured the emission-line centers and widths for the major optical emission lines that were observed with WFPC2, and these are refined in our analysis of a new spectrum in the following section. In Figure 3 we overlay the WFPC2 narrowband filter profiles on the relevant emission features in this new spectrum. Although the spectrum includes only the emission from a 2″ swath across SNR 0540, it probably captures close to the entire range of line-of-sight expansion velocities represented in the nebula. The plots show that the [S II] (F673N) and combined Hα λ6563+[N II]λ6583 (F656N + F658N) profiles capture the full velocity range of these features. The [O III]λ5007 (F502N) filter captures most of the emission but excludes some faint emission at the most extreme blue-shifted and red-shifted velocities that is likely projected against the middle of the SNR.

The WFPC2 images in Figure 1 (see also Morse 2003; Caraveo et al. 1998) reveal several Crab-like line emission properties. These images show a complex, starfish-shaped network of filaments and bubbles surrounding the synchrotron emission observed in optical continuum and X-ray emission. The remnant's [S II] emission is generally compact and filamentary, tracing out numerous arcs and protrusions. The [O III] emission likewise follows many of these features, but also hints of a more diffuse component that extends to larger radii than the [S II] emission, like an "[O III] skin" — a prominent feature in images of the Crab (Sankrit & Hester 1997). A difference image of F502N and F673N in Figure 1 shows excess [O III] emission from the outer regions of the remnant. This outer [O III] skin around SNR 0540 is most convincingly demonstrated in the 3-color image in Figure 4, where [O III] is shown in green.

Because the observed structure is very similar to what is seen in the Crab (e.g., Blair et al. 1997; Sankrit et al. 1998), we suggest that the same physical processes — e.g., ionization mechanisms, relationship between the synchrotron nebula and optical filaments, etc. — act in each of these two young SNRs. One caveat is that shock heating may be more important in SNR 0540, since our spectra indicate an electron temperature from [O III] emission that is higher than the Crab, and higher than expected for photoionization (see §4).

Another notable difference is that the *Chandra* HRC image of SNR 0540 (Gotthelf & Wang 2000; Hughes 2001) traces extended thermal emission, projected tens of arcseconds principally to the west and southwest of the SNR center, that may indicate the location of the blastwave as it interacts with the surrounding ISM. No such detection has been reported for the Crab. Unfortunately, bad luck had the WFPC2 images of SNR 0540 oriented so that the extended X-ray emission discovered later by *Chandra* fell off the WFPC2 field of view (see Fig. 2).

The bottom panels of Fig. 1 show a close correspondence between the optical (left) and X-ray synchrotron (right) emission morphologies in SNR 0540. Gotthelf & Wang (2000) speculated that the PWN is a torus of magnetized, ultrarelativistic particles oriented NE-SW, with possibly a bipolar jet extending in the orthogonal direction, similar to the structure in the Crab nebula. Sankrit & Hester (1997) present a model for the PWN in the Crab that may directly apply to SNR 0540.

4. LONG-SLIT SPECTROSCOPY

Ground-based optical spectra help to solve additional mysteries associated with SNR 0540. In a previous investigation (K89) we presented optical spectra of SNR 0540 that gave several clues to the nature of the remnant and also posed several interesting puzzles. Here we discuss new ground-based optical spectra with improved signal-to-noise ratios and higher spectral resolution, helping to confirm or clarify some results of previous studies. For the line ratios in Table 3 and throughout our discussion we assume an extinction of E(B–V) = 0.2, similar to the value of E(B–V) = 0.19 used by K89, and the reddening law of Cardelli, Clayton, & Mathis (1989). Serafimovich et al. (2004) derived a total E(B–V) = 0.2 and discuss the reddening toward the pulsar PSR B0540–69.3 in detail.

4.1. The Systemic Velocity

Narrow emission lines in the ambient H II region surrounding SNR 0540 provide a convenient way to constrain the systemic velocity of the remnant's environment, in order to check for any anomalous net motion of the remnant (see below). Table 2 lists heliocentric radial velocities measured for a 5″-long segment of the slit offset roughly 25″ northwest of the remnant center. Weighting the bright Hα line by a factor of 2, we find v_{sys}=+273.0 ±7.7 km s^{-1} for the H II region. This is different than our previous estimate of +215 ±30 km s^{-1} (K89), but is in better agreement with the mean systemic velocity of the LMC of +270 km s^{-1} (Sandage & Tammann 1981). This velocity also agrees with that deduced from UV absorption features for stars near SNR 0540, although there is a dispersion of a few dozen km s^{-1} in the observed radial velocities (Danforth et al. 2002).

4.2. Kinematics

Kinematics of emission lines can yield critical clues for understanding young SNRs like SNR 0540. Figure 5 examines the detailed kinematic structure of [O III]λ5007, the brightest line in the optical spectrum. Figure 5*a* shows the spatio-kinematic structure in the long-slit spectrum, and Figure 5*b* shows a 1-D tracing of the λ5007 line profile from an 11″ segment of the slit aperture. In both panels of Figure 5, the fainter [O III] λ4959 line has been subtracted to avoid confusion, using a shifted and scaled sample of the λ5007 line. In

our previous investigation with lower spectral resolution (K89) we found a rather high average velocity for bright emission lines in SNR 0540 of +582 ±30 km s^{-1}. This is significantly offset from the systemic velocity of the LMC, and we conjectured that the SNR 0540 progenitor may have had some net motion with respect to the LMC, or the explosion may have been asymmetric. We measure a line center at half the peak intensity of +568 ±10 km s^{-1}, in reasonable agreement with our earlier estimate. Closer scrutiny of the irregular line profile shapes in the improved data presented here, however, suggests an alternate interpretation.

The [O III]λ5007 emission shows complex structure in both panels of Figure 5. The bright core of the line forms a ring in Figure 5*a* — as expected in a kinematic cross-cut of (roughly) spherically expanding material — appearing as double-peaks at +135 and +620 km s^{-1} in the 1-D tracing in Figure 5*b*, along with a red-shifted shoulder. The center of this ring (or the midpoint between the two peaks) is at +378 km s^{-1}, which is still red-shifted by +105 km s^{-1} with respect to the surrounding environment, but far less severe than our previous estimate.

Furthermore, [O III] emission is unique among optical lines in that it also exhibits a fainter, more extended component in both position and velocity. A faint "halo" reaches to about 10″ from the star in Figure 5*a*, and a corresponding faint tail extends to high blue-shifted velocities in Figure 5*b*. Including this fainter emission, at zero intensity the [O III] emission extends from about −1400 to +1900 km s^{-1}. This previously undetected fast material has two important implications. First, the center of expansion of these extreme velocities is +250 km s^{-1}, which is consistent with *little or no net Doppler shift compared to the systemic velocity* of the surrounding H II region. This obviates the need to invoke a seriously asymmetric explosion or fast motion of the progenitor star (though see §5.1). Second, the FWZI of the [O III] line, including this fainter emission, is 3300 km s^{-1}. The faint material extends ±8″ (or a diameter of 16″ = 1.2×10^{14} km at D=50 kpc) along the slit in Figure 5*a*. This is more extended than the emission seen in our WFPC2 images, but is still only about 2/3 the size of the [O III] skin around the Crab. The corresponding dynamical age of the remnant is ∼1200 years[12], older than our previous estimate of ∼760 years (K89), and similar to the age of the Crab. The [O II]λλ3726,3729 blend does not show the faint blue-shifted tail or the red-shifted shoulder exhibited by [O III]. This implies that the red hump and the blue tail are indeed related — they may correspond to more extended faint [O III] emission than is seen in the WFPC2 images.

The qualitative similarities between the faint outer halo of SNR 0540 and the Crab nebula are remarkable; they both show roughly the same age, similar expansion speeds and similar physical sizes. The brightest inner [O III] emission around SNR 0540, however, is substantially slower and has a smaller size than the Crab. In any case, in both SNRs, the fastest material we observe in [O III] is expanding at less than about 2,000 km s^{-1} (see Figure 5 and Smith 2003). Other young SNRs, such as Cas A (Thorstensen et al. 2001), exhibit much faster ejecta with speeds of $\sim 5000 - 10,000$ km s^{-1} in the main optical shell. The difference may be due to our seeing the innermost ejecta ionized from the inside-out in SNR 0540 and the Crab, while in Cas A we see faster outer layers excited by the reverse shock.

---

[12]Note that the mass of the young remnant is probably still dominated by ejecta rather than swept-up ambient material, so the simple dynamical age may not be a severe overestimate of the true age. In addition, the expansion may be accelerated by the pulsar wind nebula, as in the Crab (e.g., Trimble 1968), which would lead to a lower age estimate than the true age.

4.3. Hα or not Hα? The 6580 Å Question

Our new spectra and those of other recent investigations (e.g., Caraveo et al. 1998) also solve a puzzle regarding the strong emission feature near 6580 Å (see Figure 6). Dopita & Tuohy (1984) suggested an identification of Ca I]λ6572.8 Å for this emission feature, since neither Hα nor [N II]λ6583 were satisifactory for this line at the systemic velocity of the LMC, although some authors have adopted either Hα or [N II] as more plausible identifications despite the wavelength discrepancies (see K89).

Our data indicate that the emission feature in question is most likely a combination of both Hα and [N II]λ6583 with comparable strengths. Figure 5*b* includes a tracing of the emission feature, plotted with respect to the heliocentric radial velocity for Hα. The emission feature in question has two strong peaks: one is red-shifted by ∼30 km s^{-1} from the systemic velocity for Hα, and the second peak coincides with the expected shift for [N II]λ6583 at the same systemic velocity (see Figure 5*b*). Additionally, there is even a faint bump near the expected position of [N II]λ6548. These data, combined with our detection of weak Hβ and the detection by Serafimovich et al. (2005) of Hβ and higher Balmer lines, confirm the presence of H and N in the SNR 0540 nebula. It is not alarming that Hα and [N II] may have different line profiles than [O III] (which is double-peaked), since the [O III] emission is seen to be spatially distinct from both [S II] and Hα+[N II] in our WFPC2 images in Figure 1. We discuss this result further in §5.

From the tracing in Figure 5*b*, the Hα/[N II] λ6583 intensity ratio appears to be ∼1.4, with an uncertainty of perhaps ±20% depending on possible differences in the individual [N II] and Hα line widths. This helps mitigate the problem of the extreme Balmer decrement of Hα/Hβ ≳20 noted previously (see K89). Correcting for the contribution of [N II] (see Table 3), we find a much lower dereddened Hα/Hβ ratio of only ∼5.3. This is still somewhat higher than the theoretical Case B value, but is not uncommon when collisional excitation of Hα is considered.

4.4. Comments on the Spectrum of SNR 0540

Figure 6 shows the optical spectrum of SNR 0540 measured in an 11″ segment of the slit, compared to the integrated spectrum of the entire Crab nebula from Smith (2003). Table 3 lists the observed and dereddened line intensities in SNR 0540. The SNR 0540 and Crab spectra are qualitatively similar. Both show strong oxygen and sulfur lines over a flat continuum of comparable relative intensity — i.e., the [O III]λλ4959,5007 equivalent widths are 344 and 300 Å in SNR 0540 and the Crab, respectively. In both remnants, the [O III] emission is spatially more extended than the continuum synchrotron nebula. Some differences in the spectra of the two remnants are that SNR 0540 has relatively weaker [Ne III], [N II], and Balmer lines than the Crab, as well as a substantially larger [O III]/[O II] ratio.

K89 estimated an electron density of $n_e \sim$ 2000 cm^{-3} in the optical nebula, though the integrated [S II]λλ6716, 6731 line profiles are complicated and difficult to deblend. Serafimovich et al. (2005) were able to deblend the [S II] lines at a few locations, finding a range of (1 – 5) ×10^3 cm^{-3}. Using this electron density, the [O III] λ4959+λ5007/λ4363 intensity ratio suggests an average electron temperature of $T_e \approx$ 25,500 K. This is less than our previous estimate of ∼34,000 K (K89), but is still within the higher temperature regime expected for shock excitation instead of photoexcitation (see also Serafimovich et al. 2005). This temperature does not rule out the possibility that photoexcitation by a hard synchrotron continuum may play an important role, but it is probably a less significant source than in the Crab where photoexcitation dominates.

The spectrum in Figure 6 shows an emission feature at ~3880 Å, which we attribute to a combination of [Ne III]λ3869, He I λ3889, and possibly H I λ3890. There may be an emission feature attributable to [Ne III]λ3968, but it is not a 3σ detection and is listed in parentheses in Table 3. Serafimovich et al. (2005) detected both lines of [Ne III]. We did not detect the [Ne III] lines in our previous study (K89), and the new detections provide some useful information for the abundance of Ne, since the [Ne III]/[O III] ratio is sensitive to abundances (see K89). The observed [Ne III]λ3869 line strength in Table 3 compared to [O III]λλ4959,5007 suggests that the relative Ne/O abundance is roughly one-third the value in the Crab nebula. The possibility of a lower Ne abundance in SNR 0540 may point to a more massive progenitor star than for the Crab, since Ne is efficiently converted to Mg for stars above 9 $M_\odot$ (e.g., Arnett 1996). Davidson & Fesen (1985) estimated a progenitor mass for the Crab of $8-10$ $M_\odot$ based on abundance measurements. A somewhat more massive progenitor in SNR 0540 may help reconcile its Crab-like qualities with the fact that it is an oxygen rich remnant. However, the SNR 0540 and Crab optical spectra stand in marked contrast to other oxygen-rich remnants in the Galaxy (Cas A; Hurford & Fesen 1996) and Magellanic Clouds (N132D, 1E 0102.2–7219; Paper 2).

5. DISCUSSION

5.1. The Outer [O III] "Skin"

High-resolution *HST*/WFPC2 images reveal for the first time a striking qualitative similarity between the emission-line morphology of SNR 0540 and the Crab nebula. In both remnants, [O III]λ5007 emission is more extended than lower ionization tracers like [S II]λλ6716,6731. In the WFPC2 images of SNR 0540, we see evidence for a faint halo of [O III] emission extending far outside the brightest inner parts of the remnant, and our spatially-resolved long-slit spectra of SNR 0540 (Figure 5*a*) trace this extended halo with a diameter of roughly 16″. In the Crab nebula, this type of morphology is thought to arise as dense filamentary supernova ejecta are overrun by the faster and lighter pulsar wind, giving rise to (magnetic) Rayleigh-Taylor instabilities (e.g., Sankrit et al. 1998). These instabilities allow the faster and higher-ionzation [O III] emission to reside at larger radii than the denser and lower-ionization knots and filaments. Based on the [O III] skin seen in our WFPC2 images, we propose that this same general scenario applies to SNR 0540 as well.

This comparison is strengthened by the similarity between the visual-wavelength spectra of SNR 0540 and the integrated spectrum of the Crab nebula as a whole (Smith 2003; MacAlpine et al. 1989). The maximum blue- and red-shifted velocities of the faint [O III] halo in SNR 0540 (roughly ±1700 km s^{-1}; see Fig. 5*b*) are similar in magnitude to the maximum [O III] velocities in the Crab. Our spectra of SNR 0540 show two distinct velocity components in the nebula: 1) a slower and brighter double-peaked feature within ±4″ of the pulsar at heliocentric velocities of roughly –100 to +900 km s^{-1}, and 2) a much faster (–1400 to +1900 km s^{-1}) and more extended (±8″) fainter component, which appears as blue and red shoulders in the extracted spectrum (Figure 5*b*). The slower and less extended component is seen in other lower-ionization optical forbidden lines like [S II], [O II], and Hα+[N II], but the faster and more extended emission is only seen in [O III]. The Crab shows both low- and high-velocity components in [O III] (Smith 2003), as well as a qualitatively similar separation of the fainter [O III] and other species in images (Sankrit & Hester 1997). However, the contrast between the two velocity components in SNR 0540 is more dramatic than in similar long-slit spectra of the Crab. The greater difference in velocities between the slow and fast components in SNR 0540 may translate to faster or stronger shocks in that remnant as the pulsar wind overtakes relatively slower material. Specifically, we suspect that shock heating in SNR 0540 causes the raised mean electron

temperature that we observe, whereas in the Crab the gas heating is dominated by photoexcitation (see §4). One could explore this hypothesis further with high signal-to-noise and high spatial-resolution spectra of [O III]λ4363 in order to derive separate electron temperatures in the slow and fast components.

The asymmetry between the blue- and red-shifted [O III] emission from the fast component in SNR 0540 is somewhat puzzling. While the extreme velocities at zero intensity are roughly symmetric about the systemic velocity of the ambient H II region (implying no severe net motion of the remnant with respect to its environment), the red shoulder is much brighter than the faint blue-shifted emission. One possible explanation for the brightness asymmetry may be that the supernova remnant is expanding into a medium with a density gradient, so that the red-shifted side of the remnant is expanding into denser material with a consequently higher emission measure. This density gradient would presumably have been caused by an asymmetric circumstellar environment created by the progenitor star. A more extreme case of asymmetry due to the surrounding material is seen in the remnant SNR 0057-7226 in the *H* II region *N66* (Danforth et al. 2003). We discuss clues about the pre-supernova circumstellar environment are further below. The asymmetry may also arise if there is asymmetry in the PWN. The optical and X-ray images (see Fig. 1) both show asymmetrical structure in the continuum emission. In addition, the pulsar proper motion measured by Serafimovich et al. (2004) may result in an asymmetrical PWN due to the net motion of the pulsar. This net motion, if confirmed, could indicate a somewhat asymmetrical explosion that may also contribute to the asymmetry in the emission and/or ejecta distribution.

Overall, however, the main result of our analysis of images and spectra is that both spatial morphology and kinematics justify a close comparison between SNR 0540 and the Crab nebula. This suggests that the global properties of the remnant can be explained by a similar model as that applied to the Crab, with a pulsar wind overtaking slower supernova debris and penetrating through the debris as a result of magneto-hydrodynamic instabilities. In our interpretation, then, the low-velocity component is composed of dense clumps of mostly supernova debris. This does not exclude the possibility that the slower component may include a contribution from swept-up circumstellar debris with different abundances that existed around the progenitor star, as discussed below.

5.2. Pre-supernova Circumstellar Ejecta?

One of the most vexing issues in SNR 0540 research is the tentative identification of emission in the 6580 Å region that may originate from a putative N-rich annulus akin to the inner ring of SN1987A. Mathewson et al. (1980) originally imaged this emission and attributed it to [N II]λ6583. Dopita & Tuohy (1984) detected broad emission spectroscopically and suggested a rare Ca I]λ6573 line as a possible origin. They reasoned that Ca is consistent with nuclear-processed material ejected from the center of the exploded star. Spectra presented by K89 also showed this feature, but they preferred Hα as the identification. However, the absence of Hβ emission in their spectra implied a Balmer decrement > 18 (when corrected for reddening), which is an equally rare phenomenon. Based on improved spectra in this paper (see also Serafimovich et al. 2005), we argued above that the feature in question is actually a blend of Hα and [N II] with complex line profile shapes, and that the addition of [N II] emission and our detection (and that of Serafimovich et al. 2005) of weak Hβ somewhat mitigates the large Balmer decrement. The presence of relatively narrow components in the spectrum led Caraveo et al. (1998) to speculate that at least some of the line-emission seen in SNR 0540 may be the remains of a N-rich ring of pre-supernova mass-loss material. Chu (2001) embraced this interpretation, noting that the emission in the F658N image is about the size of a typical luminous blue variable nebula (LBV nebulae like that around η Carinae are typically N-rich; e.g., Smith

& Morse 2004), though significantly smaller than most Wolf-Rayet bubbles. The alleged ring is now $\sim 8\times$ larger than the inner ring around SN1987A.

Caraveo et al. point out that there are significant difficulties with the pre-SN ejecta interpretation. Given the age of the SNR, the main blastwave and considerable ejecta would have impacted any such structure long ago, presumably shocking and dispersing the material. We are now seeing this process unfold in SN1987A (e.g., Michael et al. 2000; Pun et al. 2002; Sugerman et al. 2002). On the other hand, if all the material we see in WFPC2 images represents ejecta from the core of the exploded massive star, how can H and N as evidenced by our spectra be present in the very deepest layers of the evolved progenitor? By comparison, the inner filaments of the Crab are also H bearing, though unquestionably enriched. Some fast H and N knots are seen in Cas A (e.g., Fesen et al. 1987), but generally not toward the interior of the SNR.

Our proposed identification of Hα and [N II] emission in spectra (as opposed to a Ca I] feature) is consistent with the hypothesis that some of the emission associated with SNR 0540 is shocked and swept-up circumstellar ejecta that originated in the outer envelope of the star. However, based on the general emission-line morphology and especially the locations of the most prominent Hα+[N II] emitting features, not all of the low-velocity emission is pre-supernova ejecta. For example, WFPC2 images in the F656N and F658N filters show several emission knots in the inner parts of the remnant. Other nearby knots are seen in both [S II] and [O III] (with ionization levels that bracket Hα and [N II]), so the localized Hα+[N II] emission is an abundance effect and not a result of ionization properties. Thus, while some of the inner ejecta around SNR 0540 may contain swept-up N-rich gas from the circumstellar environment of the progenitor, many of the slow emission-line filaments do not. Although our observations support the idea that some N-rich ejecta around the progenitor have been swept up, our data do not allow us to constrain a specific geometry for that material, such as an equatorial ring.

In any case, the comparison between SNR 0540 and the Crab remains valid if some fraction of the inner debris originated in swept-up circumstellar material. Perhaps the scenario of a supernova remnant expanding into a pre-existing ring is *even more* applicable to the Crab. Some authors have proposed that the Crab shows putative evidence for a He-rich torus (MacAlpine et al. 1989); it has dark bays in the synchrotron nebula that remind one of a pinched waist (Fesen et al. 1992), and the global kinematics of the expansion are roughly bipolar (MacAlpine et al. 1989; Fesen et al. 1992; Smith 2003). Indeed, in drift-scan spectra of the Crab, where the [O III] emission exhibits a bipolar expansion pattern, the relatively low-velocity [O III] emission seems to reside at the waist of the bipolar expansion pattern (Smith 2003; MacAlpine et al. 1989), matching the location of the dark bays in the synchrotron nebula. SNR 0540, on the other hand, shows no clear evidence for bipolar morphology in images or in its kinematics, again casting some doubt on the hypothesis that its pre-SN ejecta resided in a ring. Rather, the overall geometry of SNR 0540 more closely resembles some "starfish" planetary nebulae, with multiple protrusions. If there had been a distinct SN 1987A-like ring around the progenitor of SNR 0540, it has since been disrupted by the expanding supernova ejecta and pulsar wind.

The authors would like to thank Jeff Hester, Joe Foy, and Rob Fesen for helpful discussions. We also thank the referee for many insightful comments that helped improve the manscript. This work has been supported under NASA grants GO-07340.01-A and HF-01166.01A from the Space Telescope Science Institute, which is operated by the Association of Universities for Research in Astronomy, Inc., under NASA contract NAS 5-26555.

REFERENCES

Arnett, D. 1996, Supernovae and Nucleosynthesis (Princeton: Princeton University Press)

Biretta, J., Lubin, L., et al. 2002, WFPC2 Instrument Handbook, Version 7.0 (Baltimore: STScI)

Blair, W. P., Davidson, K., Fesen, R. A., Uomoto, A., MacAlpine, G. M., & Henry, R. B. C. 1997, ApJS, 109, 473

Blair, W. P., Morse, J. A., Raymond, J. C., Kirshner, R. P., Hughes, J. P., Dopita, M. A., Sutherland, R. S., Long, K. S., & Winkler, P. F. 2000, ApJ, 537, 667 (Paper 2)

Caraveo, P. A., Bignami, G. F., Mereghetti, S., & Mombelli, M. 1992, ApJ, 395, L103

Caraveo, P.A., Mignani, R., & Bignami, G.F. 1998, Mem. Soc. Astron. Italiana, 69, 1061

Cardelli, J.A., G.C., & Mathis, J.S. 1987, ApJ, 345, 245

Chanan, G. A., Helfand, D. J., & Reynolds, S. P. 1984, ApJ, 287, L23

Chu, Y.-H. 2001, in Young Supernova Remnants: Eleventh Astrophysics Conf., eds. S. S. Holt & U. Hwang (AIP: New York), 409

Danforth, C.W., Howk, J.C., Fullerton, A.W., Blair, W.P., & Sembach, K. 2002, ApJ SS, 139, 81

Danforth, C.W., Sankrit, R., Blair, W.P., Howk, J.C., & Chu, Y.-H. 2003, ApJ, 586, 1179

Davidson, K., & Fesen, R. A. 1985, ARA&A, 23, 119

Dopita, M. A., & Tuohy, I. R. 1984, ApJ, 282, 135

Fesen, R. A., Becker, R. H., & Blair, W. P. 1987, ApJ, 313, 378

Fesen, R.A., Martin, C.L., & Shull, J.M. 1992, ApJ, 399, 599

Fesen, R. A., Morse, J. A., Chevalier, R. A., Borkowski, K. J., Gerardy, C. L., Lawrence, S. S., & ven den Bergh, S. 2001, AJ, 122, 2644

Gotthelf, E. V., & Wang, Q. D. 2000, ApJ, 532, L117

Hughes, J.P. 2001, in Young Supernova Remnants: Eleventh Astrophysics Conf., eds. S. S. Holt & U. Hwang (AIP: New York), p. 419

Hurford, A. P., & Fesen, R. A. 1996, ApJ, 469, 246

Kirshner, R. P., Morse, J. A., Winkler, P. F., & Blair, W. P. 1989, ApJ, 342, 260

MacAlpine, G.M., McGaugh, S.S., Mazzarella, J.M., & Uomoto, A. 1989, ApJ, 342, 364

Mathewson, D. S., Dopita, M. A., Tuohy, I. R., & Ford, V. L. 1980, ApJ, 242, L73

Michael, E., et al. 2000, ApJ, 542, L53

Middleditch, J., Pennypacker, C.R., & Burns, M.S. 1987, ApJ, 315, 142

Morse, J.A. 2003, RMxAC, 15, 243

Morse, J. A., Blair, W. P., Dopita, M. A., Hughes, J. P., Kirshner, R. P., Long, K. S., Raymond, J. C., Sutherland, R.,S., & Winkler, P. F. 1996, AJ, 112, 509 (Paper 1)

Pun, C.S.J., et al. 2002, ApJ, 572, 906

Sandage, A., & Tammann, G. A. 1981, *Revised Shapley-Ames Catalog of Bright Galaxies* (Carnegie Inst. of Washington, Publ. 635)

Sankrit, R., et al. 1998, ApJ, 504, 344

Sankrit, R., & Hester, J. 1997, ApJ, 491, 796

Serafimovich, N.I., Shibanov, Y.A., Lundqvist, P., & Sollerman, J. 2004, A&A, 425, 1041

Serafimovich, N.I., Lundqvist, P., Shibanov, Y.A., & Sollerman, J. 2005, in Proc. 35th COSPAR Scientific Assembly, in press (astro-ph/0501523)

Seward, F., Harnden, D., & Helfand, D. 1984, ApJ, 287, L19

Smith, N. 2003, MNRAS, 346, 885

Smith, N., & Morse, J.A. 2004, ApJ, 605, 854

Sugerman, B.E., Lawrence, S.S., Crotts, A.P.S., Bouchet, P., & Heathcote, S.R. 2002, ApJ, 572, 209

Thorstensen, J. R., Fesen, R. A., & van den Bergh, S. 2001, AJ, 122, 297

Trimble, V. 1968, AJ, 73, 535

Table 1. HST-WFPC2 Observations of SNR0540–69.3

Filter	λ_{mean}[a] (Å)	$\Delta\lambda$[a] (Å)	Exposure Time (s)	Observation Date
F502N	5012.4	26.9	$2 \times 1300{,}6 \times 1400$	17 October 1999
F656N	6563.8	21.5	$2 \times 700{,}3 \times 1000$	19 October 1995
F658N	6590.8	28.5	3×1000	19 October 1995
F673N	6732.2	47.2	$2 \times 1300{,}4 \times 1400$	17 October 1999
F336W	3329.3	374.3	2×300	17 October 1999
F547M	5467.8	483.2	2×400	17 October 1999
F555W	5336.8	1228.4	2×300	19 October 1995
F791W	7811.2	1230.7	2×200	17 October 1999

[a]Values for the mean wavelength and effective filter bandpass width are taken from the Cycle 10 WFPC2 Instrument Handbook.

Table 2. Wavelengths and Velocities in the H II Region

λ Observed (Å)	I.D.	λ Air (Å)	Radial Velocity (km s^{-1})
4105.5	Hδ	4101.7	+278
4344.6	Hγ	4340.5	+283
4865.8	Hβ	4861.3	+278
4963.6	[O III]	4958.9	+284
5011.4	[O III]	5006.8	+273
5881.1	He I	5875.6	+281
6306.2	[O I]	6300.3	+281
6553.8	[N II]	6548.0	+266
6568.6	Hα	6562.8	+265
6589.3	[N II]	6583.5	+264
6722.4	[S II]	6716.4	+268
6736.7	[S II]	6730.8	+263

Table 3. Optical Emission Spectrum of SNR 0540–69.3

Wavelength (Å)	I.D.	EW (Å)[a]	Observed F[b]	Dereddened F[b]
3726,3729	[O II]	154	36.1	45.8
3869,3889	[Ne III],He I[c]	19.0	4.4	5.5
3968	[Ne III]	(4.7)	(1.1)	(1.3)
4069,4076	[S II]	11.5	3.0	3.6
4363	[O III]	10.6	2.9	3.3
4861	Hβ	4.7	1.4	1.4
4959,5007	[O III]	344	100	100
5876	He I	3.8	1.1	1.0
6300	[O I]	13.5	3.8	3.3
6364	[O I]	4.1	1.1	0.9
6548,6563,6583	Hα,[N II]	65.1	17.2	14.5[d]
6716,6731	[S II]	150	40.8	33.8

[a]Emission-line equivalent width is positive. Uncertainty is roughly 20% for faint lines, and a few percent for the stronger lines.

[b]Relative line intensities are given on a scale with [O III] λ4959+λ5007 = 100.0. In our calibrated spectra through a $2''\times11''$ aperture, the observed [O III] $\lambda\lambda$4959,5007 flux is 4.7×10^{-14} ergs s^{-1} cm^{-2}, and the dereddened intensity is 8.9×10^{-14} ergs s^{-1} cm^{-2}. Dereddened fluxes are for $E(B-V) = 0.2$ and R_V = 3.1 using the reddening law of Cardelli, Clayton, & Mathis (1989).

[c]Weak H I λ3890 may also be present in this blend.

[d]The Hα/[N II]λ6583 ratio is $\sim$1.4, so we estimate that the individual dereddened intensities on a scale of [O III] = 100 are [N II]λ6548 $\approx$ 1.8, Hα $\approx$ 7.5, and [N II]λ6583 $\approx$ 5.2.

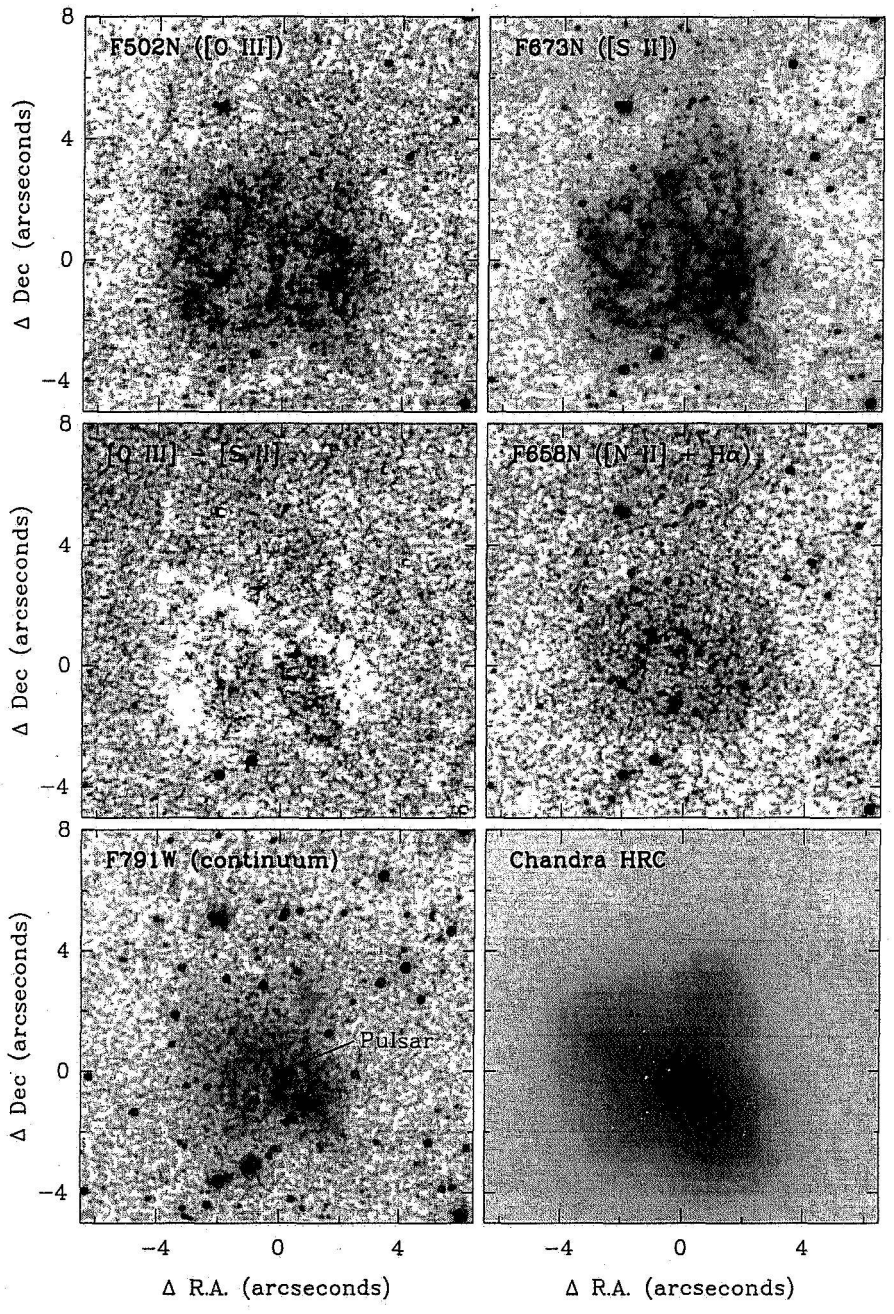

Fig. 1.— Close-ups of the high-resolution *HST*/WFPC2 Planetary Camera and *Chandra* HRC images. (a) F502N [O III] λ5007; (b) F673N [S II] $\lambda\lambda$6716,6731; (c) [O III] − [S II] difference image, relatively strong [O III] emission is white; (d) F658N [N II] λ6583 and red-shifted Hα; (e) F791W red continuum; and (f) *Chandra* HRC image (Gotthelf & Wang 2000). The pulsar candidate is identified in the continuum image in panel (e).

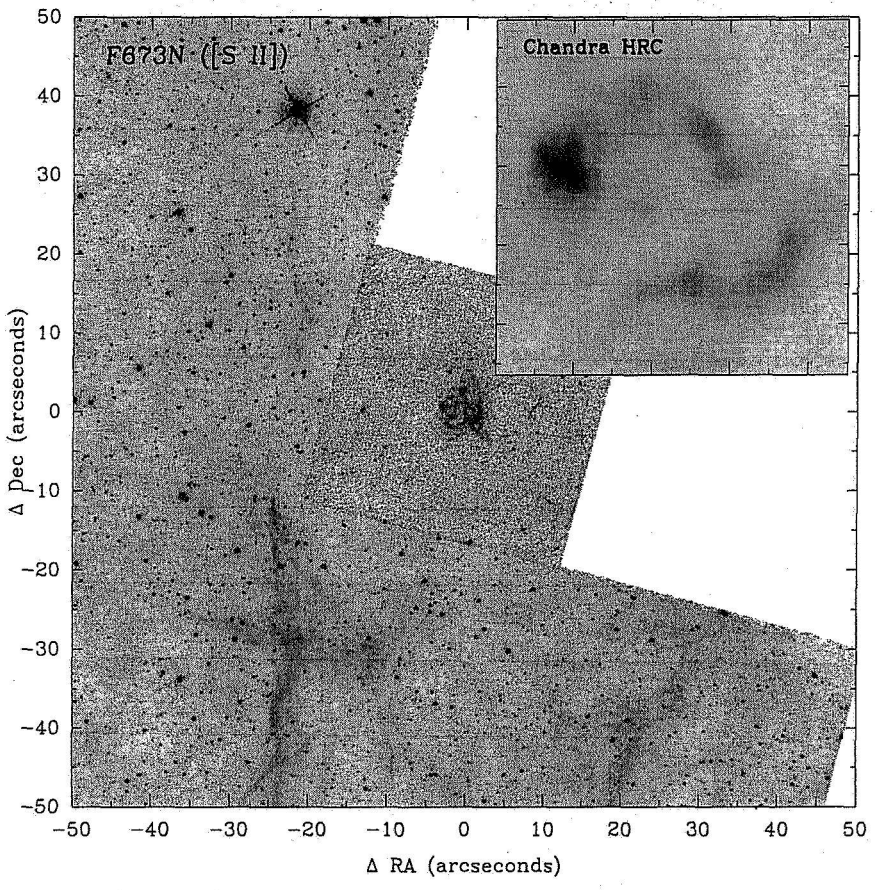

Fig. 2.— A portion of the WFPC2 F673N image mosaic showing the environment surrounding SNR 0540. Unfortunately, the shape of the WFPC2 field of view and available guide stars resulted in the extended X-ray emission later seen in the *Chandra* HRC map (inset, Gotthelf & Wang 2000) falling within the zone of avoidance.

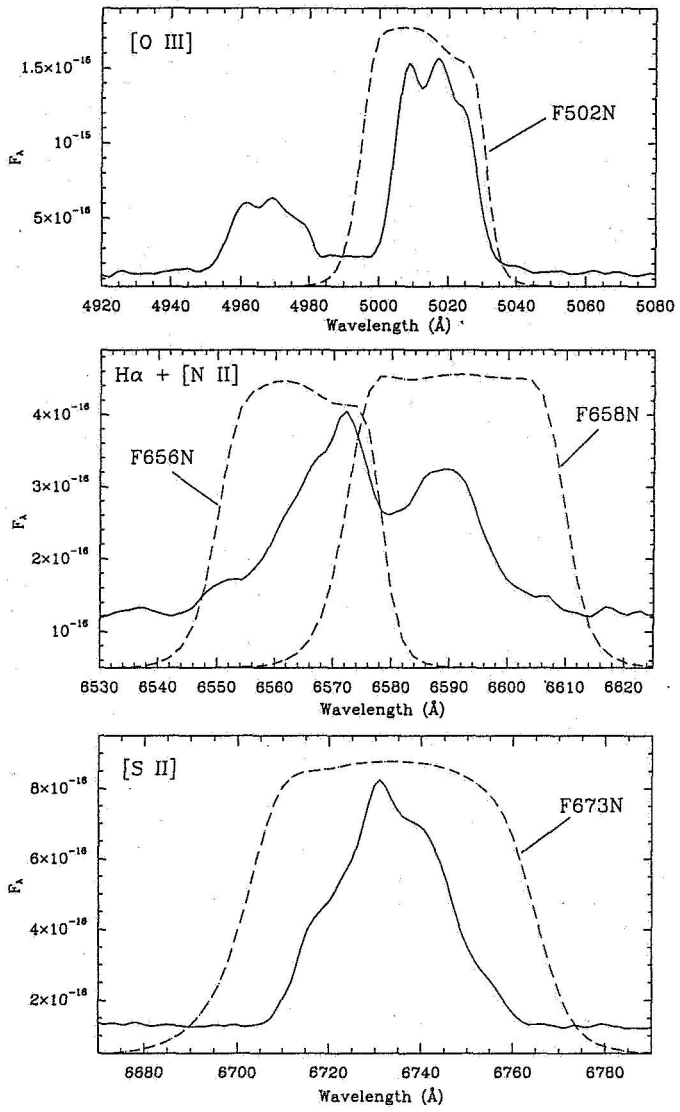

Fig. 3.— WFPC2 narrowband filter profiles overlaid on the relevant emission lines in the spectrum presented in Fig. 6. The F673N and combined F656N+F658N filters capture the full extent of the [S II]λ6716, 6731 and Hα+[N II]λ6583 emission, but the F502N filter misses some of the most extreme blue-shifted and red-shifted [O III]λ5007 emission.

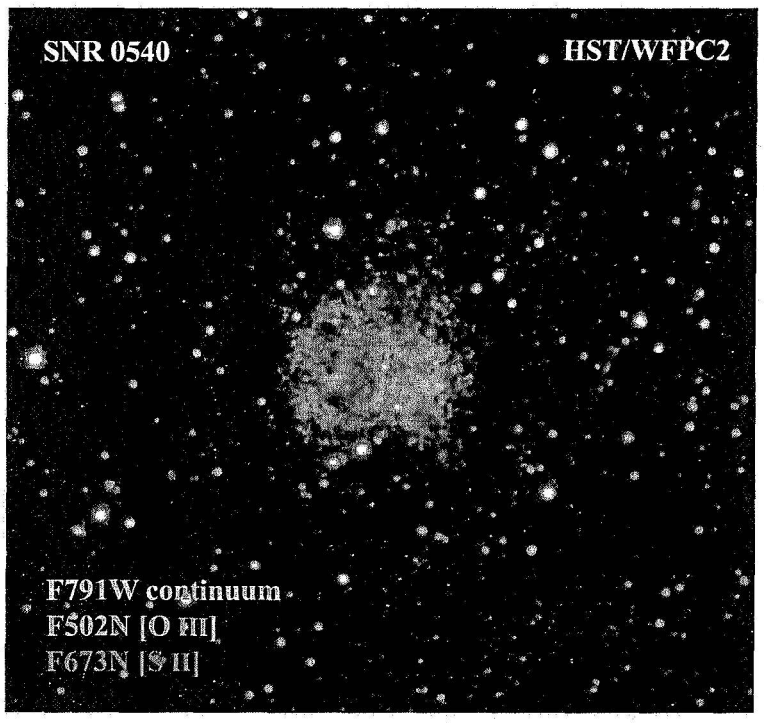

Fig. 4.— A 3-color WFPC2-PC image of SNR 0540, with the F791W continuum emission shown in blue, [O III]λ5007 in green, and [S II]$\lambda\lambda$6716, 6731 in red. The field of view is $28\farcs6 \times 26\farcs6$ with north to the top and east to the left.

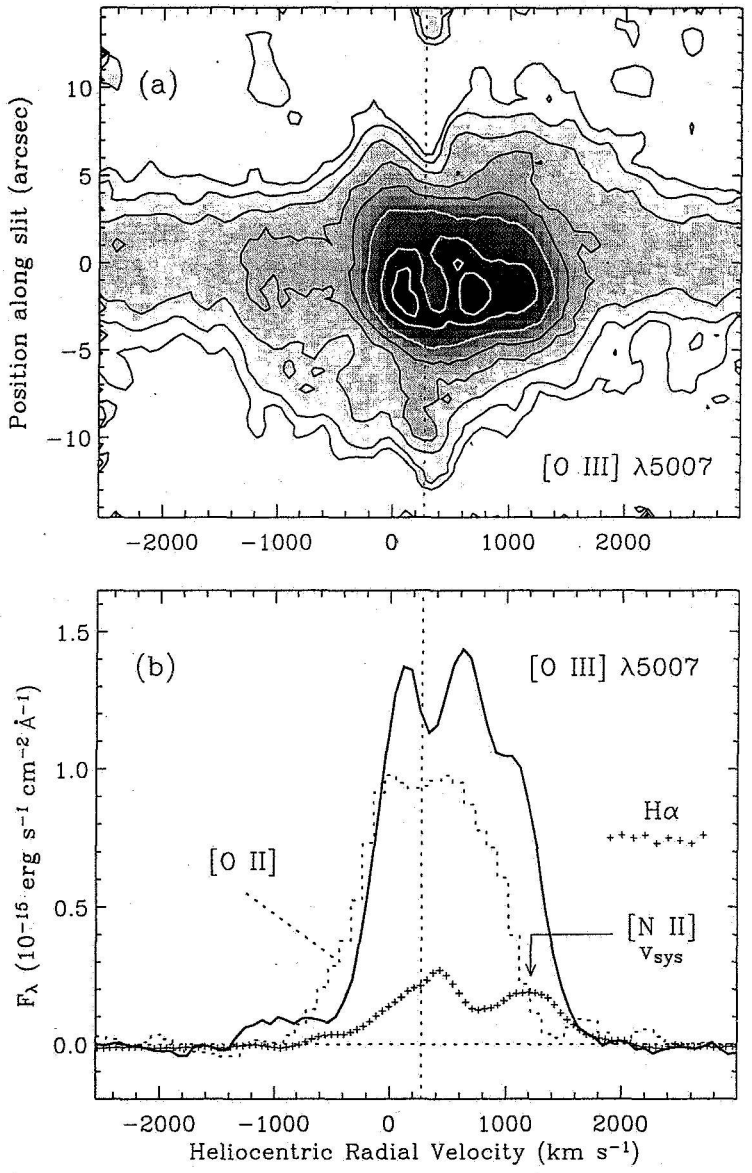

Fig. 5.— (a) Spatio-kinematic structure of the [O III]λ5007 line from SNR 0540-69.3. (b) Tracing of the line profile of [O III]λ5007 (solid line) compared to the combined [O II]λλ3726,3729 profile (dotted histogram) and the Hα + [N II]λλ6548,6583 blend plotted relative to the heliocentric velocity for Hα. In both panels, the [O III]λ4959 line has been removed by shifting, scaling, and subtracting the λ5007 line profile. The vertical dashed line in each panel shows the measured heliocentric velocity of the ambient H II region, v=+273 km s^{-1}, taken to be the systemic velocity. In panel (b), the dashed horizontal line at zero is the subtracted continuum level of 1.36×10^{-16} ergs cm^{-2} s^{-1} Å^{-1}. The small arrow in panel (b) indicates the expected location of the systemic velocity of [N II]λ6583 relative to Hα.

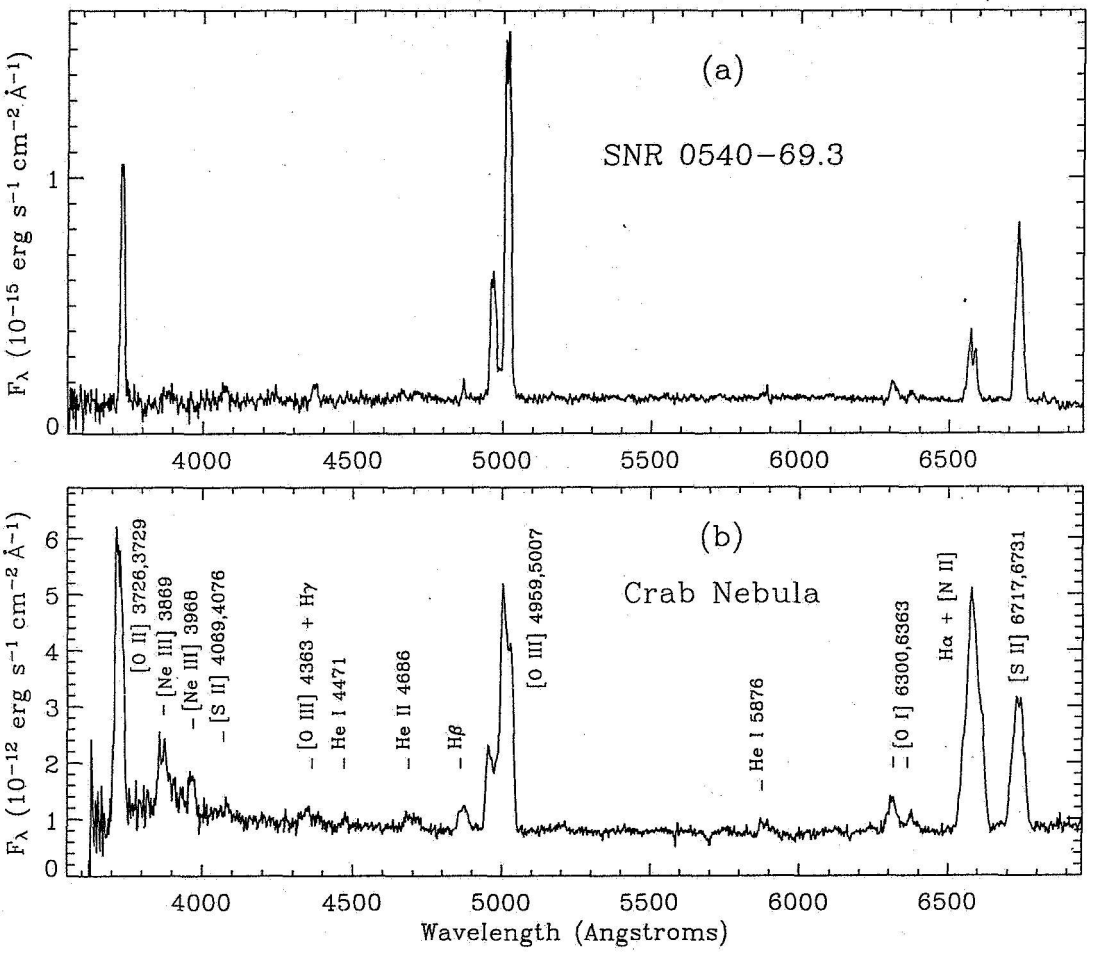

Fig. 6.— (a) Spectrum of SNR 0540-69.3 observed through a $2'' \times 11''$ aperture. For comparison, panel (b) shows the integrated optical spectrum of the entire Crab nebula from Smith (2003).